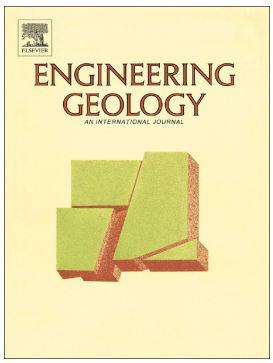

Analysis of major rock slides that occurred during the 2016–2017 Central Italy seismic sequence

Giovanni Forte, Luca Verrucci, Anita Di Giulio, Melania De Falco, Paolo Tommasi, Giuseppe Lanzo, Kevin Franke, Antonio Santo

PII: S0013-7952(21)00205-2

DOI: https://doi.org/10.1016/j.enggeo.2021.106194

Reference: ENGEO 106194

To appear in: *Engineering Geology*

Received date: 31 July 2020

Revised date: 30 January 2021

Accepted date: 13 May 2021

Please cite this article as: G. Forte, L. Verrucci, A. Di Giulio, et al., Analysis of major rock slides that occurred during the 2016–2017 Central Italy seismic sequence, *Engineering Geology* (2021), https://doi.org/10.1016/j.enggeo.2021.106194

ANALYSIS OF MAJOR ROCK SLIDES THAT OCCURRED DURING THE 2016-2017 CENTRAL ITALY SEISMIC SEQUENCE

Giovanni Forte[1,*], Luca Verrucci[2], Anita Di Giulio[3], Melania De Falco[1], Paolo Tommasi[3], Giuseppe Lanzo[2], Kevin Franke[4], Antonio Santo[1]

[1]Dipartimento d'Ingegneria Civile, Edile e Ambientale; Università degli Studi di Napoli Federico II, Naples, Italy
[2]Dipartimento d'Ingegneria Strutturale e Geotecnica, Sapienza Università di Roma La Sapienza, Rome, Italy,
[3]CNR – Istituto di Geologia Ambientale e Geoingegneria, Rome, Italy
[4]Department of Civil and Environmental Engineering, Brigham Young University, Provo, UT, USA

[*]Corresponding author.

Abstract

The 2016 Italian seismic sequence was characterized by three main shocks that occurred on August 24th, on October 26th and 30th. The latter, a *Mw* 6.5 event, is the strongest seismic event recorded in Italy since the 1980, *Mw* 6.9 Irpinia Earthquake. In this time span between the first and the third shock of the 2016 sequence, more than 1,000 seismic events of *Mw* greater than 3.0 and shallow hypocentral depth between 7 and 11 km were recorded, triggering more than of 1,300 observed landslides. In this paper, the identification of the triggering models for four selected rock slides was performed together with the mechanical characterization of the affected rock masses both in situ and in laboratory. Large scale morphostructural setting was analyzed to verify the role of regional tectonics in the failures. Discontinuity sets were identified at detail-scale using three-dimensional (3D) point clouds developed from structure from motion (SfM) reconstruction using unmanned aerial vehicles (UAVs). In situ and laboratory tests coupled to data from UAV 3D models were used for geomechanical characterization. Data were finally adopted as input of limit equilibrium static analyses, which allowed a better comprehension of the stability conditions prior to seismic events and clarify some aspects of the mobilized strength.

Keywords: Rock slides; Earthquakes; Point Clouds; Central Italy; UAV.

1. INTRODUCTION

The 2016-2017 Central Italy seismic sequence triggered more than 1,300 landslides identified through on-site surveys and interpretation of aerial photographs. Most of these landslides are rock falls and rock slides, similar to the landslides that have occurred in historical earthquakes in the same area (**Guzzetti et al. 2009**). During the seismic sequence, all landslides except the retaining wall failure documented in Pescara del Tronto (**Lanzo et al., 2019; Franke et al., 2019**) were structurally controlled, and originated on steep and high slopes, formed by jointed rocks. These events can be mainly classified as Category I "Disrupted Slides and Falls" by **Keefer** (**1984**) classification that includes highly to very highly disrupted landslides consisting of boulders and masses of rock fragments and translational sliding. The described scenario is consistent with what is reported by **Rodrıguez et al. (1999)** in a review paper on seismic-induced landslides. Only a few rock slides involved more than 100 m^3 of material and evolved into small rock avalanches (**Tommasi et al. 2019**), impacting adjacent infrastructure and touristic footpaths of the Sibillini Mts. National Park, which luckily were not frequented due to the late fall season.

Rock slope failures represent one of the most significant forms of ground failures caused by moderate to strong earthquakes (*Mw* 5.0 to 7.0), and they have caused significant damage worldwide in recent years. For example, the 2011 Canterbury, New Zealand *Mw* 7.1 earthquake and its ten *Mw* > 5.0 aftershocks triggered thousands of rock falls in the Port Hills of Christchurch, which led to the evacuation of hundreds of families (**Massey et al., 2014**). Similarly, the coseismic rock falls triggered on Lefkada Island by the 2015 Lefkada, Greece *Mw* 6.5 earthquake completely covered the majority of the west coast beaches and damaged access roads (**Kallimogiannis and Saroglou, 2019**). The study and the analysis of rock slope failures such as the examples presented here can be performed using four progressive stages according to the scale of investigation and the complexity of the methodologies used (e.g. **Silvestri et al. 2016** and papers referenced therein).

The 2016 Italian seismic sequence was characterized by three main shocks that occurred on August 24th (Accumoli earthquake, *Mw* 6.0), on October 26th (Visso earthquake, *Mw* 5.9) and October 30th (Norcia earthquake, *Mw* 6.5). The entire sequence was characterized by seven shocks with *Mw* higher than 5.0 (**Tab. 1**) and lasted 5 months in duration. It strongly affected the small town of Amatrice and other several municipalities in four different administrative regions (Lazio, Abruzzo, Umbria and Marche), causing more than three hundred casualties and heavily damaging many historic buildings of heritage as well as the physical environment (**Miano et al., 2020** and papers referenced therein). Over the course of the 5-month sequence, more than 1,000 seismic events of *Mw* > 3.0 and shallow hypocentral depth between 7 and 11 km were recorded. **Fig. 1** presents the mapped locations of the main shocks and aftershocks along with their temporal evolution as they advanced in northward direction until December 2016 and then finished with the final occurrences in January 2017 in a southward direction near the city of L'Aquila and the Abruzzo Region. **Table 1** presents the orientations obtained from time domain moment tensor solutions for the seismogenic fault segments activated by each event. Generation of strongest shocks involved one or more

segments of the SW dipping normal dip-slip faults belonging to the Laga Mts.-Mt.Bove-Mt.Vettore alignment.

In the aftermath of the 2016 seismic sequence, several research groups mapped more than 800 landslides involving road cuts in rock and fill slopes over an area of about 2000 km^2 (**GEER, 2016**; the Institute for environmental protection and research **ISPRA, 2016**; the Centre for Prediction, Prevention and Control of Geological Risks by Roma La Sapienza). These data are summarized in the CEDIT catalogue (**Martino et al., 2017**), where almost 150, 250 and 420 seismic slope displacements were identified after the August 24th, October 26th and October 30th earthquakes, respectively. Successively, the Authors (**DICEA-RELUIS, 2018**) identified from Google Earth™ imagery an additional 550 landslides, as shown in **Fig. 1**.

This study aims to characterize typical failure models of large, wedge-type seismic-induced rock slides to: *i)* investigate the role of large scale morphostructural setting, *ii)* understand the stability conditions prior to seismic events and *iii)* clarify some aspects of the mobilized strength. To these aims, remote structural measurements, laboratory investigation and quantitative data on rock mass structure and joint surface conditions (e.g. rock bridge area, roughness) were retrieved from high-resolution three-dimensional (3D) point cloud models developed from aerial photographic surveys using small unmanned aerial vehicle (UAV) surveys performed after both the August 24th and October 30th shocks.

Detailed data and evidence of these types of rock failures are not common in the earthquake literature, especially regarding occurrences in Italy, which are usually just generically reported as "rock falls" without defining mechanisms and/or structural/geomechanical data. In this paper, we introduce the geological and seismological setting of the area affected by earthquakes (section 2) and the historical record of earthquake triggered landslides in the area (section 3). Details regarding four representative large rock slides at large and small scales are presented (section 4), and analysis results are shown (section 5) and discussed (section 6).

2. GEOLOGICAL AND SEISMOLOGICAL SETTING

The geological setting of the area affected by the 2016 seismic sequence is characterized by several stratigraphic and tectonic units from Lias to Miocene (more details in **Pierantoni et al. 2013** and referenced papers). The simplified geological sketch in **Fig. 2a** reports massive or coarsely-bedded limestones (CB) mainly belonging to *Calcare Massiccio Fm.,* underlying several stratified marly-calcareous rocks, namely *Corniola Fm., Marne del Monte Serrone Fm., Rosso Ammonitico Fm., Calcari e Marne a Posidonia Fm.* and *Calcari Diasprigni Fm.* of Jurassic age (McB). The Cretaceous-Oligocene sequence starts with *Maiolica Fm.,* which is a medium-thin bedded pelagic limestone and that stratigraphically passes to more marl-rich deposits such as *Marne a Fucoidi Fm., Scaglia (Rossa, Bianca, Variegata, Cinerea) Fms., Bisciaro Fm.* and *Marne a Pteropodi* and *Cerrogna Fm.,* which are all included in the McB geologic unit presented in the geologic map shown **Fig. 2a**. Conversely, clayey (CFB) and arenaceous flysch deposits (AFB) mainly crop

out in Laga Mts. together with conglomerates (CgB) (**Fig. 2a**). The study area was affected by multi-phased contractional and extensional deformations consistent with the geologic formation of Italy.

Quaternary post-orogenic extension is superimposed on a Neogene fold-and-thrust belt developed after the collision of the African and European continental margins. Thrust faulting was preceded by pre-orogenic extension phases that resulted in three major structural trends striking NE, NNE and E(SE), defined as anti-Apennines systems. After the main compressive phase, the area was definitively uplifted and the compressive structures were dissected by NW-SE striking (Apennines trend) normal faults during the Quaternary (**Cello et al., 1997; Boncio and Lavecchia, 2000, Pizzi and Galadini, 2009** and references therein). The intermountain depressions (e.g. Colfiorito, Castelluccio, Norcia, Cascia, Spoleto, Foligno, etc.) were formed during the Quaternary extensional phase due to extensional tectonics and the combined effects of two anti-Apennines systems (NNE–SSW and ENE–WSW), the latter acting with trans-tensional mechanisms (**Calamita and Pizzi, 1993**). The geomorphologic setting of the area is strongly controlled by structural features and lithology. The former control is apparent in the drainage network, which is influenced by the structural pattern as the main drainage lines are located along the trace of the main regional faults. The latter can be found in the distributions of the slope angle (i.e., high steep ridges that are made of calcareous rocks and more gentle slopes corresponding to the flysch deposits.) Alluvial and lacustrine deposits (shown as db, tcg, gs in **Fig. 2a**) are found in the intra-mountain basins. These deposits can reach a thickness of more than 100 m and are formed by the interlayering of lower-middle Pleistocene gravels, clays and sands. Finally, travertine deposits (shown as tv in **Fig. 2a** and dating from the middle Pleistocene up to now) are also readily found in the region. They are mainly formed by spring water whose chemical content is connected to the activity of deep faults and fractures (**Quattrocchi et al., 2000**).

Within a 5-month period, the 2016 seismic sequence involved approximately 1500 km^2 of the regional normal fault system (**Barani et al., 2017**; **Tinti et al., 2016**) over an area of seismic gap between the 1997 *Mw* 6.1 Colfiorito-Sellano earthquakes to the north and the 2009 *Mw* 6.1 L'Aquila earthquake to the south (**Chiarabba et al., 2009**; **Chiaraluce et al., 2004**). Source mechanisms of the shocks that occurred during the 2016 sequence, including both after- and fore-shocks with moment magnitude within the range 5.0-5.5, were analysed based on seismological data (**Chiaraluce et al. 2017**). Analysis of GPS and InSAR data from the three main shocks allowed further insight into source mechanisms. The *Mw* 6.0 August 24th shock was generated by the rupture of two fault segments: the northern part of the SW dipping Mt. Gorzano - Laga Fault (GLF- **Fig. 2a**) and of the southern part of the Mt. Vettore-Bove Fault (VBF) (**La Vecchia et al., 2016**). The rupture mechanism of the October 30th *Mw* 6.5 is much more complex. **Cheloni et al. (2017)** notes that the rupture process involved a normal fault antithetic to the VBF and/or a low angle thrust plane re-utilized with extensional kinematic. Similarly, **Scognamiglio et al. (2018)** used inversion of recorded ground-velocity waveforms and co-seismic GPS displacements to observe that coseismic rupture occurred

along a normal fault plane of the VBF fault with dip direction of 245° and a segment of the Sibillini thrust fault dipping at 36° towards WNW.

3. PAST LANDSLIDES IN THE STUDY AREA

Over the last 2,000 years, a number of seismic events with ground motion intensity approaching XI MCS (Mercalli-Cancani-Sieberg macroseismic scale) impacted the study area (CPTI15.2 catalogue, **Rovida et al. 2019**) and triggered several documented landslides. The most reliable dataset of earthquake-induced landslides was collected after the 1997 Colfiorito-Sellano seismic sequence that was comprised of six shocks with *Mw* ranging from 5.0 to 6.0 (**SGA, 2000; Esposito et al., 2000**; **Antonini et al., 2002**). Except for the large rock slide that occurred in Serravalle del Chienti during the 1279 earthquake (estimated *Mw* 6.2), which involved an estimated 1,000,000 m^3 of rock (**Boschi et al., 1997 in Antonini et al., 2002**), most of the recorded landslides are rock falls, topples and small rock slides as well as rotational slides in debris deposits. However, when historic landslides were non-destructive, historical sources only reported morphological changes and surface ruptures from which landslide occurrence can be inferred. Data collected after the 1997 earthquake by **Esposito et al.** (**2000**) and **Guzzetti et al.** (**2009**) report that about 90% of the 250 documented landslide events are rock falls, topples and small rock slides up to a few tens of m^3 in volume. According to **Antonini et al.** (**2002**), rock slides were also triggered by aftershocks of relatively small moment magnitude. Conversely, the 2016-2017 central Italy seismic sequence triggered a total number of 1370 landslides: 170 after the Accumoli shock, 400 after the Visso shock, and 800 events after the Norcia shock. These events can be mainly classified within the "Category I - disrupted slides and falls" of Keefer's classification (**Keefer**, **1984**) (**Fig. 2b**). These categories encompass phenomena of very different type and extent: rock and soil falls, rock planar and wedge slides, rock and soil avalanches (**Hungr et al. 2014**). Similar to past landslides, many small/shallow slope failures occurred after the 2016 August 24th earthquake, mainly affecting limestones and subordinately the sandstone units on high steep slopes, road cuts and sides of road embankments, and terraced deposits. Conversely, the landslides resulting from the 2016 October shocks affected the regional highway running through the lower Valnerina (**Boschi et al., 1997; Esposito et al., 2000**) along a stretch of the Nera valley. Rock slides were small and only under specific stratigraphic conditions (interbedding of sound and poorly cemented travertines) did they ever achieve a few thousands of m^3 of material (**Esposito et al., 2000**). Similar observations were made with the slope and retaining wall that failed at Pescara del Tronto during the 2016 August 24th event (**Franke et al. 2018**).

In this paper, geomechanical, structural and kinematic characterization were performed for four case studies representative of large rock slides selected from the available inventoried landslides (**Table 2**). Their location is reported in **Fig. 2a** and the frontal view from UAV-based digital surface models is shown in **Fig. 3**.

The selected landslide case histories were triggered at epicentral distances ranging from 2.3 km to 16.8 km (**Table 2**) and affected the Carbonate and Marly Carbonate units of the bedrock, in particular the geological formations known as *Calcare Massiccio* (Early Jurassic) and *Maiolica* (Early Cretaceous). **Table 2** also presents the following estimated ground motion characteristics corresponding with the horizontal component of maximum PGA of each triggering earthquake: peak accelerations, mean periods according to **Rathje et al.** (**1998**), and significant durations between 5% and 95% of the Arias Intensity. These reported ground motions at the case study sites were estimated for a horizontal rigid outcrop using ground motion prediction equations (GMPE) based on Italian data (**Bindi et al., 2011**) as well as interpolating the available ground motion recordings from the nearest accelerometric stations on rock (**Verrucci et al., 2021**).

4. METHODOLOGY

Instability mechanisms of the selected landslides were reconstructed through large- and local-scale studies. The former consisted of interpreting the morphostructural setting, while the latter consisted of merging traditional field surveys and laboratory testing with advanced remote sensing methods that employed rapid and low-altitude aerial imaging from UAVs and 3D reconstruction from structure from motion computer vision (SfM) approaches (see also **Franke et al., 2018**).

4.1 Large scale investigations

In the vicinity of each landslide, a large-scale study of the morphostructural setting was performed. The aim of this study was to identify the dominant orientation of morphostructural features and faults to relate them with joint systems surveyed in the scars of the landslides (local scale approach). The landslides were located on a 1:25.000 topographic map and the strikes of fault segments were reported over a radial area of 10 km. The landslides were taken from the official geological maps and from morphostructural evidence using aerial photographs as morphologic alignments, presence of escarpments, subsequent valleys, ridges and anomalies of the hydrographic network. The length of the segments was arbitrarily assumed equal to 1 km, so that persistent regional faults were divided into more segments; in this manner, the same statistical weight was attributed to each segment. Fault strike distribution was plotted as rose diagrams.

4.2 Local scale investigations

The first task was to identify the seismic event that triggered the collected landslides (**Fig. 2 and Table 2**). To this purpose accounts by local witnesses were verified with observation of Google Earth™ "historical" images, which proved to be invaluable in constraining the date of the events on slopes that are located far from infrastructure and/or population centres. In some cases, images were processed through filters to extract valuable visual information and to enhance them.

4.2.1 UAV investigations

The detailed analysis of each landslide scar (see **Fig. 3**) conducted through advanced UAV-based aerial 3-D imaging permitted the creation of 3D models developed using Structure from Motions (SfM) computer vision techniques. The aerial imaging was primarily performed with the DJI™ Phantom 4 quadrotor UAV platform. It was equipped with a 4K video camera that has a 1/2.3" CMOS sensor, 94-degree field of view, 12.4 MP images, and a focal length of infinity. UAVs were first flown autonomously such that nadir images from a specified altitude (usually at least 10 meters from the surface of the ground) with a minimum image overlap of 70% in both the horizontal and forward directions were captured. UAVs were then flown manually to capture oblique imagery and video from various altitudes.

Captured images were processed and reconstructed with SfM techniques (**Marr and Nishihara 1978**; **Snavely et al. 2008**). SfM incorporates tie point extraction using a scale invariant feature transform (SIFT) algorithm (**Lowe 2004**) with known camera internal parameters to develop a sparse point cloud on a local coordinate system. Surveyed ground control points (GCPs) and check points (CPs) were used to anchor the sparse point cloud and reference it to global coordinates. Bundle block adjustment was performed to minimize location error in the sparse point cloud. Once adjusted, the sparse point cloud was populated with a dense point cloud using a variant of the semi global matching approach proposed by **Hirschmüller** (**2005; 2008**). Upon completion of the dense point cloud, various model products were developed including a three-dimensional meshed model, digital surface model (DSM), digital elevation model (DEM), and orthorectified aerial images of the rock slides. Finally, point clouds were manually adjusted using the freeware *CloudCompare* v2.10.2, which enabled the removal of "floating" points and the cropping/resizing of the models around the landslide/rockfall scars. The extraction of major landslide discontinuities was performed using the 3D dense point clouds using the *CloudCompare* Facets plug-in (**Dewez et al. 2016**) subsampled to an average ground nearest distance (GND) of 2 cm. The Facets plugin extracts geological planar features from the 3D point clouds, calculating dip and dip direction. The plugin divides the point cloud into clusters of adjacent points sharing some user-defined degree of coplanarity. Two different approaches based on a least-square fitting algorithm (**Fernandez 2005**) were adopted: a) Kd-Tree (Kd) and b) Fast Marching (FM) method. The space subdivision in Kd was observed to be irregular. Fortunately, the space subdivision in FM was observed to be regularly divided. Elementary subdivisions were back-clustered together according to a coplanarity criterion, resulting in set of flat polygons adjusted to match the size and geometry of the original 3D point cloud. Each polygon was defined as a mesh with a contour, an extent, a centroid, and a normal.

Processing and interpretation of UAV-based 3D point cloud models permitted to collect information regarding volume and shape of the failed rock mass including area of the surfaces forming the scar, joint spacing and persistence. UAV data require a certain degree of user expertise to correctly identify the orientation of joint sets (dip/ dip direction) and surface conditions of discontinuities controlling failure kinematics (second order roughness, waviness, presence and extent of rock bridges possible alteration of surfaces). At Piè la Rocca (PR), results were verified on the basis of in situ measurements of the attitude of bedding and major discontinuities taken within the scar. At Sasso Pizzuto rock slide in the Nera Gorge (NR),

orientation and roughness of a few major discontinuities belonging to the main sets were measured immediately uphill from the landslide scar during a rope access survey. On site measurements were subsequently used to calibrate the remote structural analysis. The obtained discontinuity sets were compared with the main fault sets identified with the morphostructural setting of the region. Costa Cattiva (CC) and Rubbiano (RB) sites as well as at the lower part of the Sasso Pizzuto rock slide (NR) were completely inaccessible and UAV data were the only source of structural and geomechanical information.

4.2.2 Geomechanical investigations

To obtain information on rock properties and assess the strength parameters, rock samples taken from rockfall deposits in *Calcare Massiccio Fm.* and *Maiolica Fm.* were collected. Laboratory testing involved triaxial tests, uniaxial compression tests, tensile tests, and elastic wave velocity (pulse tests). The results of these tests are necessary for performing slope stability analyses (**Verrucci et al. 2021**).

Shear strength parameters of the rock discontinuities that controlled the failures were estimated with reference to the modified Barton criterion for continuous joints (**Bandis 1990**), which accounts also for large-scale undulations:

$$\tau_p = \sigma_n \tan\left[\varphi_r + JRC_n \log_{10}\left(\frac{JCS_n}{\sigma_n}\right) + \omega\right] \quad (1)$$

where σ_n is the normal stress acting on the joint, φ_r is the residual friction angle representing the non-dilative strength component, JRC_n; and JCS_n accounts for roughness and compressive strength of the joint surface at the block size; and ω is the inclination of large-scale undulations along the direction of sliding. Information on joint roughness at medium- to large-scale was obtained from the analysis of dip-parallel profiles of discontinuities, extracted from UAV 3D point cloud models. To obtain this information the resolution of the models must be sufficiently high to allow accurate interpretation of the rock joints. The average GSD (ground surface distance) of the rock slide SfM models employed in this study is 2.1 cm (developed from photographs with resolutions ranging from 5.6 mm/pixel to 31 mm/pixel). This accuracy is more than sufficient to determine large-scale undulation angles (ω) and major angle asperities at block scale.

At Sasso Pizzuto (NR) and Rubbiano (RB), failure involved intact rock bridges, along joints, or small surfaces where the fractured rock mass was sheared. These new ruptures in turn provided further contribution to the mobilized resisting forces, either in shear or in tension, depending on the landslide kinematics (i.e., on the slide direction respect to the portion of failure surface where rupture of fresh rock has been observed). In particular, patches of fresh ruptures have been identified on close-up images of the two failure scars in the form of spots of fresh rock along joints or irregular surfaces throughout the rock mass. Their contribution to the resisting forces has been estimated by calculating the area of fresh rock patches attributed to the rock bridges (A_p) or to the rock mass involved in the failure (A_b) multiplied by the strength of the rock bridges or that of the rock mass, respectively (see section 5).

4.2.3 Slope stability analyses

Static back-analysis slope stability assessments on simplified models were performed using the limit equilibrium method with the assumption that wedges are only subjected to gravity forces. Any potential water pressure in the joints was excluded. We believe this assumption is valid because: a) the slopes in question have high dip angles, thus reducing infiltration; b) high rock mass permeability allows rapid drainage; and c) rainfall in the days preceding the landslides was not intense nor prolonged (25 to 32 mm in the 10 days preceding the landslides) to saturate the joints. A Mohr-Coulomb failure criterion was assumed to represent shear strength along the wedge surfaces. Strength parameters are reported in **Table 3** and geometrical parameters in **Table 4** with Safety Factors.

5. RESULTS

The results of the analyses to characterize the mechanical and geometrical features of the case studies are reported for each rock slide in **Fig. 3**. The analysed cases primarily affected limestone formations known as *Calcare Massiccio Fm.* (Early Jurassic) and *Maiolica Fm.* (Early Cretaceous), as summarized in **Table 2**.

Mechanical properties of *Maiolica Fm.* and *Calcare Massiccio Fm.* were measured from specimens cored from blocks retrieved from the landslide deposits. Uniaxial compression tests, tensile tests, and elastic wave velocity (pulse tests) were conducted on both lithotypes, while triaxial tests were conducted only on specimens from the *Maiolica Fm*. A summary of the results of laboratory tests is reported in **Table 3** with corresponding estimates of the local *GSI* (Geological Strength Index) values.

Differences in *GSI* between the different areas depend primarily on the intensity of jointing. Where closely spaced bedding joints are present throughout the whole rock mass (as at NR and CC sites), *GSI* is rather homogeneous within the rock mass. At the PR site, bedding joints are rarer, but fracture spacing varies widely. At the RB sites, both bedding and fracture spacing are quite variable. These variabilities in turn cause the *GSI* to be more variable, as well as local measured shear strength values and shear wave velocity.

Unpublished data on small-scale strength of rock joints and on dynamic stiffness for both lithotypes collected during previous investigations campaigns at neighbouring sites were also examined. We determined φ_r in expression (1) from both tilt tests on saw-cut limestone surfaces (i.e., base friction angle) and from direct shear tests on natural joints by subtracting the dilation component, φ_{dc}, from the shear strength angle (**Hencher and Richards, 2015**). Both procedures yielded values of φ_r in the range 30°-32°.

The average values of JRC_0 (base length of 0.1 m) and the Schmidt hammer rebound height R_L determined at the Nera Gorge site on the joints of set J_1, along which sliding mostly occurs (see section 5.1), are 3 and 42, respectively. The estimate of JCS_0 from rebound height R_L, which accounts for actual joint surface conditions better than the compressive strength from intact specimens, was based on a correlation between pairs of rebound height and *UCS* values measured on the same core sample (**Fig. 4**) for lithotypes of the Umbria-Marche sequence. This curve was preferred to the abacus by **Miller** (**1965**) because the latter

overestimates UCS respect to that measured on actual specimens. An average JCS_0 of 35 MPa was obtained. JRC_0 and JCS_0 were scaled to the average spacing of the bedding joints (i.e., about 1 m) through the relationship proposed by **Barton et al.** (**1985**), resulting in: JCR_n=1.8÷3.3 and JCS_n=26.5÷30.5 MPa.

Undulations ω were reconstructed through profiles generated with the *CloudCompare* code on dense point clouds by intersecting the sliding surfaces with orthogonal planes parallel to the direction of sliding. For NR, CC and PR rock slides, the average angle of large-wavelength undulations along 10-m long stretches is 12° for major joints of the WSW-ENE trending set (range is 7°- 21°) and 6° for major joints of the N-S trending set (range is 2°- 9°). At the Rubbiano rock slide, undulations were estimated on the N-S trending major joints, which were the only joints in which sliding is kinematically possible and hence shear strength can be mobilized.

The cohesion and tensile strength provided by the rock mass (c_b and σ_{tb}) and the cohesion provided by rock bridges c_p in the *Maiolica Fm.* can be estimated from the Hoek-Brown (HB) criterion (**Hoek & Brown, 1980**) using the linearization proposed by **Hoek et al** (**2002**). For the rock mass the highest value of the disturbance factor (D = 1) has been chosen, which accounts for the severe state of relaxation at the rock cliff and the large time it has been acting for. For the NR rock slide, c_b can be estimated in 60 kPa, assuming a GSI of 55, whilst at RB site, σ_{tb} provided by the rock mass delimiting the wedge at its back can be estimated in about 60 kPa assuming a GSI of 50. More uncertain is the estimate of c_p for the NR rock slide. In fact c_p ranges between the cohesion of the intact rock material (some 2 MPa) and that of a slightly fractured rock mass (0.53 MPa assuming GSI=85). The lower bound accounts for some damage of the rock bridges, which seems to be reasonable at the scale of the extent of the bridges along the joints.

In the following sub-sections, the local geological setting for each case study is shown together with the main faults and the inferred morphostructural features. The 3D models of the scar area are reported, highlighting the main discontinuity sets and the stereoplots with Fisher concentrations of poles and related great circles. Results of the large-scale morphostructural analyses are discussed and compared with those from structural analyses on the detailed 3-D models of the rock slides. Finally, preliminary limit equilibrium back analyses of the rock slides are presented.

5.1 Nera rock wedge-slide (NR)

The Nera rock-slide (NR) shown in **Fig. 3a** affected Sasso-Pizzuto Mt. and was the largest of the failures we investigated. Its debris dammed the Nera River and subsequently blocked the flow of traffic on a major highway between the eastern and western portions of Central Italy. The landslide is a rock wedge-slide that affected the *Maiolica Fm.* as shown in **Fig. 5a**. In the same figure, the main normal faults (Plio-Pleistocene) and morphostructural features are also reported and are mainly trending N150-160. The outcrop is intensely bedded: bedding joints are less than 1m-thick and dip against the slope. The wedge detachment was controlled by the intersection of very persistent discontinuities. After the failure, the mass movement evolved into a rock avalanche with an estimated volume deposit between 32,000 m^3 (**Franke et al., 2018**) to 46,000

m^3 (**Romeo et al., 2017**). Wedge geometry was determined by calculating the orientations of the sliding surfaces and reconstructing the original cliff surface from the 3D model. The remote structural analysis of the point cloud is shown in **Fig. 5b**, which highlights the three main joint sets. Fisher concentrations of dip/dip direction of each facet are shown in **Fig. 5c**. The rock wedge moved along the intersection of systems J1 and J2, which plunges at 60°. They have an average orientation of 75°/335° (J1), 63°/284° (J2) and 78°/106° (J3); the pole density of the latter set is less evident. Bedding is oriented 48°/95°, i.e. dipping against the slope; the orientation was measured on site because it could not be inferred from the point cloud model. During the demolition/recovery works on the cliff, joint orientations and joint surface conditions were verified with rope access surveys supported by experienced rock climbers.

5.2 Costa Cattiva wedge-slide (CC)

The Costa Cattiva (CC) rock wedge-slide shown in **Fig. 3b** detached from the southern flank of the Nera River valley approximately 2 km east from Visso and fell into the Nera River, threatening the SP-134 highway after a runout of 150 m. The slide is a rock wedge similar to a prism affecting the thin-bedded limestones of *Maiolica Fm.* (**Fig. 6a**). It is the closest case study to the epicentre of the October 30th main shock and is characterized by an estimated material volume of 400 m^3 (**Tommasi et al., 2019**). Sliding occurred along the intersection of discontinuity J1 (75°/335°) and J2 (35°/090°), plunging at about 50°, and daylighting at low-angle on the slope (**Figs. 6b-6c**). The sliding plane J1 is similar to those of the J1 set found at the NR site (75°/335°), dipping toward northwest at very high angle. The failure was controlled by local joint systems superimposed on the main tectonic setting. The rock wedge resulted inclined at a value of 30°.

5.3 Piè la Rocca rock wedge slide (PR)

On the northern slope of Mount Patino (**Fig. 7a**), approximately 5 km northeast from Norcia, the August 24th earthquake triggered several landslides having considerable run-out (up to 400 m). They encroached on some forestry roads and hiking trails. The largest event of Piè La Rocca (PR) (**Fig. 3c**) mobilized about 15,000 m^3 of limestone (*Calcare Massiccio Fm.*) with a wedge-sliding mechanism. The area was also almost certainly affected by the October 30th earthquake, considering the short source-to-site distance (around 2 km). The Mount Patino area has historically been prone to earthquake-induced landslides. For example, investigations conducted by **SGA** (**2000**) discovered evidence of prior rock falls on the mountain flanks during the 1858 earthquake.

After an initial planar sliding, the rock wedge crumbled down the slope northwards, knocked down large trees and fragmenting into blocks up to 1,500 m^3 in volume. UAV surveys that we performed revealed many open joints at the top of the crown that isolate large blocks in precarious stability conditions. **Figure 7b** presents the 3D point cloud model of the scar. The surfaces of the wedge have an area of 470 m^2 and 980 m^2, respectively. In this case, three main joint sets were identified: J1 (70°/ 345°), J2 (72°/106°) and the

sliding surface B (45°/270°) corresponding to the bedding, (**Figs. 7b – 7c**). The J1 system seems to be a recurrent local discontinuity set that is also responsible for the kinematics of the NR and CC landslides. The intersection between the two systems plunges at 55°.

5.4 Rubbiano rock-slide (RB)

The Rubbiano (RB) rock-slide (**Fig. 3d**) occurred at the foot of a steep gorge flank (Infernaccio Gorge) in the eastern part of Sibillini Mts., where the layered limestone of *Maiolica Fm.* overlies the calcareous marls of the *Scaglia Fm.* through an apparent thrust plane. The geological setting is quite complex due to its location in a fold-deformed area (**Fig. 8a**). The main Plio-Pleistocene faults are NNE-SSW oriented, with a subordinate trend representative of the recurrent N140-150 Apennine direction (**Fig. 8a**). The rock slide, located just above the tectonic contact, produced a scar extending over 4,000 m^2 and a landslide deposit of approximately 15,000 m^3 (**Franke et al., 2018**). The 3D point cloud model obtained by processing UAV images (**Fig. 8b**) suggests that an irregular wedge slid along a major discontinuity characterized by an orientation of 65°/084° (J2). The crown area falls in a fold, hence it is possible to identify two main bedding sets representative of the flanks, i.e. B1 60/297 and B2 46/263. The back of the wedge is a complex surface with average orientation composed by a mosaic of joints belonging to different sets, including the J1 (85°/310°), J2 (65°/084°) and J3 (72°/010°). The latter shows an attitude similar to the bedding at Piè la Rocca site (PR), with a wedge inclination of 65° (**Fig. 8c**).

6. DISCUSSION

The 2016 seismic sequence triggered around 1,370 landslides. Approximately half of these slides occurred on road cuts and involved small volumes (from less than 1 m^3 to a few m^3). The remaining slides occurred on natural rock slopes and mobilized volumes ranging from a few tens to a few tens of thousands of m^3. Landslides mostly involved the Mesozoic limestones and the sandstone layers of the *Laga flysch Fm*. Few events involved quaternary weak rocks (breccias, conglomerates and travertines) (**Dicea-Reluis, 2018**). Epicentral distances (**Table 2** and **Fig. 2**) fall within 40 km, below the upper bound of the epicentral distance versus the surface wave magnitude curve by **Keefer** (**1984**). The largest societal impact of the documented landslides induced by the 2016 seismic sequence was the damage to transportation infrastructure and the prolonged closure of traffic. The occurrence of rock falls and small rock avalanches on a few main highways and arterials prevented vehicular travel along routes for periods of time ranging from a few weeks to several months. The longest road closure involved the State Route 209 "Valnerina" that opened on February 1st 2018, nearly one year and half after the occurrence of the NR rock slide. Restoration costs exceeded 10 million euros and included the removal of unsafe boulders, restoration of old wire-rope fences, construction of new flexible barriers for the protection of the roadway, construction of a temporary junction, removal and re-profiling of the collapsed mass, demolition of a tunnel, reconstruction of a bridge and eventually the

reconstruction of the riverbed of the Nera River. Hence, the post event management was mainly affected by the increase of the travel times required to travel along an alternative path on limited high mountain roads.

For all studied rock slides, analyses of point clouds from remote surveys provided a high quantity of dip/dip direction measurements that were characterized by higher dispersion. Significant portions of certain models were poorly represented by the UAV-based point clouds due to the unfavourable exposure/visibility of the outcrop. Both of these issues required expert judgement to integrate the point cloud model with in situ traditional surveys.

The results of the large-scale morphotectonic study were compared to the discontinuity sets identified on UAV imagery and 3D point clouds taken within the rock slide scars and are presented in **Fig. 9**.

The rosette plots (**Figs. 9a-9c-9e-9g**) represent radial histograms of strike frequency of the identified faults and morphostructural features (**Figs. 5a-6a-7a-8a**). This analysis highlighted a high-frequency NNW-SSE system that is the Apennines trend originated during the Quaternary. The N-S and anti-Apennines NE-SW systems area less frequent in the geostructural setting as they represent older deformation stages. In **Figs. 9b-9d-9f-9h**, the stereonets plots of the great circles of the main discontinuity sets of the rock wedge detachments are reported. The comparison highlights that older anti-Apennines systems played a relevant role in the wedge detachment: the NE-SW trending system, identified with J1, is a high-angle (70°-85°) recurrent system that is always associated to the J2 system, a N-S trending set dipping either toward East or West at angles ranging between 35° and 72°. Other local systems, namely J3 or bedding (B), also contributed to form the wedge surfaces either as single major joints or in combination with the other systems. A close examination of UAV models indicates that major joints belonging to the N-S trending set are smooth even at a scale considerably larger than the block size. These features imply that the shear strength angle was not much higher than the sum of the φ_{dc} value from DS tests and the inclination ω of large-scale undulations, the contribution of second order asperities being quite small. Observation of close pictures of the slide scars taken from 3D point clouds indicates that major discontinuity surfaces delimiting the failed rock mass present clear evidences of rock bridges, in the form of whiter and rougher patches (**Fig. 10**).

Fig. 11 shows simplified geometrical models of the rock slides. The reconstruction of the NR wedge is also in agreement to the model proposed by **Romeo et al.** (**2017**), who considered this rock slide to be the largest that has occurred in the area during the last two centuries.

The simplified geometrical models (**Fig. 11**) were adopted to perform static stability back-analyses and to calculate the safety factor, F_s. As deduced from Section 5, the friction angle on the sliding planes varies between 40° and 47° depending on the local roughness and waviness.

The contribution as joint cohesion of the portions of intact rock failed during sliding, evaluated according to the procedure described in section 5. Input parameters, sliding mechanisms and safety factors are shown in **Table 4**.

The PR wedge was close to limit equilibrium conditions without assuming the presence of bridges of intact rock along the surfaces of the failure scar.

The RB wedge was close to limit conditions under static loading even assuming the contribution (in tension) of a noticeable area of rock mass at the back of the wedge. This resisting area would have been successively broken by seismic shaking with the consequent detachment of the rock wedge. This is also indirectly confirmed by back analyses discussed in the paper by **Verrucci et al.** (**2021**). The failure plane delimiting the wedge at the back is a mosaic of several joints belonging to different sets, which can be interpolated with a plane oriented 85°/130°. To ensure the equilibrium of the wedge in static conditions, this surface likely provided a tensile strength, estimated through the Hoek-Brown criterion (see section 5).

For the Nera rock slide (NR), static equilibrium is not satisfied without a noticeable cohesive contribution due to portions of intact rock along the surfaces of the failure scar. Cohesion, c_p, provided by rock bridges along joint J1 should have exceeded 600 kPa to ensure equilibrium ($F_s \geq 1$). This implies that rock bridges were formed by scarcely fractured rock (GSI between 85 and 90) or rock material for a large extent (see section 5). A further hypothesis is that the wedge was not completely isolated by joints J1 and J2 (they both looks like dead-end joints on the UAV images) but a spur of fractured rock at its tip could have provided supplementary shear strength, in addition to that along the two joints. This hypothesis is suggested by the irregular shape of the lower corner of the slide scar surface and by its pale colour, typical of failure in fresh rock (**Fig. 11a**). Multiplying the value c_b calculated in section 5 by the area of failure surface passing throughout the spur, A_{b1}, F_S ranges between 1.0 and 2.23 for a cohesion of the rock bridges varying between 0.53 and 2 MPa. The area A_{b1} measured on the 3D model from UAV data (see section 4.2.2) is equal to 800 m^2.

The sliding mechanisms in static limit equilibrium conditions are controlled by the direction of the resultant external force, i.e. the block weight. The spherical surface representing the totality of the space directions possibly assumed by the resultant force can be divided into regions (spherical triangles) corresponding to different mechanisms (**Londe at al., 1969, Goodman et al., 1985**); these regions have vertexes defined by the vectors normal to the sliding planes and the lines of intersection of the same sliding planes. For the examined rock slides, the mechanism regions are reported in the stereographic projection of the lower hemisphere (upper focal point) together with the position of the weight force (red circle symbols) in **Fig. 12**. It is evident that in the cases of Nera (NR) and Piè la Rocca (PR) the resultant force in static conditions falls close to the boundary between two different mechanisms: the sliding along a single plane and the sliding along an intersection line between two planes. Therefore, small deviations of the resultant force (i.e., as imposed by an earthquake) or minor modifications of the plane orientations can produce a change in the mechanism.

The examined cases all regard highly asymmetric wedges, which are characterized by low values of F_s under sliding conditions due to the reduced strength of one of the sliding surfaces. Furthermore, failure occurred at the top of secondary ridges that arise from the average trend of the valley flank. These ridges were

susceptible to ground motion amplifications from both the fundamental frequency of the slope and the higher frequencies associated with the earthquake motions themselves (**Verrucci et al., 2021**). Strong ground motions from other shocks of significant magnitude in the seismic sequence likely also influenced the triggering of these landslides, given that numerous such shocks occurred during the seismic sequence over a period of five months.

7. CONCLUSIONS

The analysis of rock slide initiation triggered by the 2016 Central Italy seismic sequence described in this paper leads to several main conclusions:

- The studied rock slides are representative of the most affected geologic formations by the seismic sequence, i.e. *Calcare Massiccio Fm.* and *Maiolica Fm.*, and were studied by merging classical methods with newer remote sensing approaches. In particular, UAV-based point cloud models produced by SfM methods permitted us to obtain much more information regarding the rock cliffs (dip/dip direction) and their associated joint conditions (roughness, persistence) that would otherwise not have been possible due to inaccessibility and/or safety concerns.
- Structural analyses on the 3D point clouds provided a high quantity of dip/dip direction measurements as well as a higher dispersion. This means that the correct interpretation of the failure mode requires an expert judgement to highlight significant sets that were poorly represented by the point cloud models alone.
- The four examined rock slides were largely controlled by the geostructural setting at the scale of the slope. In fact, all the cases are characterized by the presence of major discontinuities of the older anti-Apennines sets (NE-SW) despite their representation at relatively smaller scales due to the much higher frequency of the quaternary Apennines tectonic sets (NW-SE).
- Stability analyses indicate that rock slide resulted in very precarious conditions in both the static and dynamic cases; hence, any observed cases of stability can only by justified by the presence of rock bridges that are reinforcing the strength of the entire rock mass. These bridges were broken during the seismic shaking, resulting in the triggering of the rock slides. Evidence of these rock bridges can be seen in the point cloud models as white or lighter patches on the scarp surfaces. The extent of these patches was estimated using the point cloud models.
- Although remote sensing methods for mapping discontinuities have improved in recent years, remote detection of intact rock bridges on cliff faces remains challenging and should be further addressed in future research, as their existence is typically confirmed only *after* failure (i.e., white patches in the scar area).
- The studied failures occurred at the top of secondary ridges that rise from the average trend of the valley flank. They tend to be impacted by ground motion amplification from both the fundamental

frequency of the slope and higher frequencies associated with the earthquake itself. This is another challenging issue associated with the seismic stability of rock cliffs, which, together with the cyclic response of the rock masses, resulted in a gradual and sequential breakage of the rock bridges as the 2016 seismic sequence continued over a period of five months.

ACKNOWLEDGEMENTS

Thanks are due to Eng. Valerio Sabatini and Eng. Davide D'Alberti for the Piè la Rocca UAV survey. Eng. Marco Mancina (ANAS, National Highways Dept.) provided assistance and data for the Nera River Valley. Mr. Luca Imperio is greatly acknowledged for the support to rope access survey. The Authority for the Sibillini Mts. National Park is gratefully acknowledged for giving permission of conducting surveys in the park area. UAV flight permits and access to several landslide areas were obtained thanks to the help of Engg. Paola Pagliara and Paola Bertuccioli of Dipartimento della Protezione Civile. Eng. Valentina Tuccio carried out preliminary seismic response analyses for the Nera River Valley. Thanks are extended to the Brigham Young University undergraduate students Brandon Reimschiesel, Bryce Berrett, Nicole Hastings, Jeff Derricott, Brigette Ostrem Valdez, Doug Graff, and graduate student Michael Freeman for expertly operating the UAVs at these various landslides.

FUNDING

The research was partially funded by the Italian Civil Protection Department RELUIS project (2018), PR8-UR18-WP2 UNINA (Principal investigator A. Santo) and by Progetto di Ateneo Sapienza 2017 "Site investigations, monitoring and modelling of earthquake induced rock slides triggered by the 2016 Central Italy seismic sequence" (Principal investigator G. Lanzo). The work was partially carried out within the activity of GEER Association, which is supported by the National Science Foundation (NSF) through the Geotechnical Engineering Program under Grant No. CMMI-1266418. This work was also partially supported by the Center for Unmanned Aircraft Systems (C-UAS), a National Science Foundation Industry/University Cooperative Research Center (I/UCRC) under NSF Award No. CNS-1650547 (Co-Principal Investigator K. Franke). P. Tommasi benefitted from EmerTer Project funded by Italian D.P.C. (Principal Investigator M. Moscatelli). Research financial support was generously provided for the Brigham Young University students by a 2018 Mentored Research Grant (MRG) provided by the Ira A. Fulton College of Engineering.

Author statement

Giovanni Forte: Conceptualization, Methodology, Validation, Formal analysis, Investigation, Resources, Data Curation, Writing - Original Draft, Writing - Review & Editing; **Luca Verrucci:** Validation, Formal analysis, Investigation, Resources, Data Curation, Writing - Original Draft, Writing - Review & Editing,

Visualization; **Anita Di Giulio:** Formal analysis, Investigation, Resources; **Melania De Falco:** Validation, Formal analysis, Investigation, Writing - Review & Editing, Visualization; **Paolo Tommasi:** Conceptualization, Methodology, Validation, Investigation, Resources, Writing - Original Draft, Writing - Review & Editing, Supervision, Project administration, Funding acquisition; **Giuseppe Lanzo:** Supervision, Project administration, Funding acquisition; **Kevin W. Franke:** Methodology, Investigation, Resources, Data Curation, Writing - Review & Editing, Project administration, Funding acquisition; **Antonio Santo:** Conceptualization, Methodology, Validation, Formal analysis, Investigation, Writing - Review & Editing, Supervision, Project administration, Funding acquisition.

REFERENCES

Antonini G., Ardizzone F., Cardinali M., Galli M., Guzzetti F., and Reichenbach P. (2002). Surface deposits and landslide inventory map of the area affected by the 1997 Umbria-Marche earthquakes. Bollettino Società Geologica Italiana, 121:2, Special Volume 1, 843–853.

Bandis S.C. (1990). Mechanical properties of rock joints. Int. Symp. on Rock joints, Loen, Norway, N.Barton & O. Stephansson (eds.), Balkema, Rotterdam, 125-140.

Barani S., Mascandola C., Serpelloni E., Ferretti G., Massa M., Spallarossa D. (2017). Time–Space Evolution of Seismic Strain Release in the Area Shocked by the August 24–October 30 Central Italy Seismic Sequence. Pure and Applied Geophysics, 174, 1875–1887.

Barton N., Bandis S.C., Bakhtar K., (1985). Strength, deformation and conductivity coupling of rock joints. Int. J. Rock Mech. Min. Sci., 22, 121-140.

Bindi D., Pacor, F., Luzi, L., Puglia, R., Massa, M., Ameri, G., Paolucci, R., (2011). Ground motion prediction equations derived from the Italian strong motion database. Bull Earthquake Eng (2011) 9:1899–1920, doi:10.1007/s10518-011-9313-z.

Boncio P., Lavecchia G. (2000). A geological model for the Colfiorito earthquakes (September-October 1997, Central Italy). Journal of Seismology, 4, 345–356.

Boschi E., Guidoboni E., Ferrari G., Valensise G., Gasperini P. (1997). Catalogo dei forti terremoti in Italia dal 461 a. C. al 1990, Pubbl. ING-SGA-ING Rome, Italy, 951 pp. (in Italian).

Calamita F., Pizzi A., (1993). Tettonica quaternaria nella dorsale appenninica umbro–marchigiana e bacini intra-appenninici associati. Studi geologici Camerti Camerino sp. Proc. Conf., 92, 17–25 (In Italian).

Cello G., Mazzoli S., Tondi E., Turco E. (1997). Active tectonics in the Central Apennines and possible implications for seismic hazard analysis in peninsular Italy. Tectonophysics 272, 43–68.

Cheloni D., De Novellis V., Albano M., Antonioli A., Anzidei M., Atzori S., Avallone A., Bignami C., Bonano M., Calcaterra S., Castaldo R., Casu F., Cecere G., De Luca C., Devoti R., Di Bucci D., Esposito A., Galvani A., Gambino P., Giuliani R., Lanari R., Manunta M., Manzo M., Mattone M., Montuori A., Pepe A., Pepe S., Pezzo G., Pietrantonio G., Polcari M., Riguzzi F., Salvi S., Sepe V., Serpelloni E., Solaro G., Stramondo S., Tizzani P., Tolomei C., Trasatti E., Valerio E., Zinno I., Doglioni C. (2017). Geodetic model of the 2016 Central Italy earthquake sequence inferred from InSAR and GPS data. Geophysical Research Letters, 44: 6778-6787, doi:10.1002/2017GL073580

Chiarabba C., Amato A., Anselmi M., Baccheschi P., Bianchi I., Cattaneo M., et al. (2009). The 2009 L'Aquila (Central Italy) M_W 6.3 earthquake: Main shock and aftershocks. Geophysical Research Letters, 36, L18308. https://doi.org/10.1029/2009GL039627

Chiaraluce et al. (2017). The 2016 Central Italy Seismic Sequence: A First Look at the Mainshocks, Aftershocks, and Source Models. Seismological Research Letters, 88(3): 757-771.

Chiaraluce L., Amato A., Cocco M., Chiarabba C., Selvaggi G., Di Bona M., et al. (2004). Complex normal faulting in the Apennines thrustand- fold belt: The 1997 seismic sequence in central Italy. Bulletin of the Seismological Society of America, 94(1), 99–116. https://doi.org/10.1785/0120020052

Dewez T.J.B., Leroux J., Morelli S. (2016). Cliff collapse hazard from repeated multicopter UAV acquisitions: return on experience. The International Archives of the Photogrammetry, Remote Sensing and Spatial Information Sciences, Volume XLI-B5, 2016.

Dicea – Reluis (2018). Report delle Attività svolte nel I semestre. PR8-UR18-WP2-UNINA, (in Italian).

Esposito E., Porfido S., Simonelli A.L., Mastrolorenzo G., Iaccarino G. (2000). Landslides and other surface effects induced by the 1997 Umbria–Marche seismic sequence. Engineering Geology, 58, 353–376.

Fernández, O. (2005). Obtaining a best fitting plane through 3D georeferenced data. Journal of Structural Geology, 27(5), 855-858.

Forte G., Chioccarelli E., De Falco M., Cito P., Santo A., Iervolino I. (2019). Seismic soil classification of Italy based on surface geology and shear-wave velocity measurements. Soil Dynamics and Earthquake Engineering, 122, 79 – 93.

Franke K.W., Lingwall B.N., Zimmaro P., Kayen R.E, Tommasi P., Chiabrando F., Santo A. (2018). Phased reconnaissance approach to documenting landslides following the 2016 Central Italy Earthquakes. Earthquake Spectra, 34, 4, 1693-1719.

GEER (2016). Engineering reconnaissance following the 2016 M6.0 Central Italy earthquake. Report n.o GEER-050A. Geer Team Leaders: Eds. J.P.Stewart and G.Lanzo. doi:10.18118/G65K5W.

GEER (2017). Engineering reconnaissance following the October 2016 Central Italy earthquake. Report n.o GEER-050D. Geer Team Leaders: Eds. P.Zimmaro and J.P.Stewart. doi:10.18118/G6HS39.

Goodman R E, Shi G, (1985). Block theory and its applications to rock engineering. Prentice-Hall Inc., Englewood Cliffs, New Jersey.

Guzzetti F., Esposito E., Balducci V., Porfido S., Cardinali M., Violante C., Fiorucci F., Sacchi M., Ardizzone F:, Mondini A., Reichebach P., Rossi M. (2009). Central Italy seismic sequences-induced landsliding: 1997-1998 Umbria-Marche and 2008-2009 L'Aquila cases, The Next Generation of Research on Earthquake-induced Landslides: An International Conference in Commemoration of 10th Anniversary of the Chi-Chi Earthquake, 2009, 52-61.

Hencher S.R., Richards L.R. (2015). Assessing the shear strength of rock discontinuities at laboratory and field scales, Rock Mech. Rock Eng., 48:883–905.

Hirschmüller H. (2008). Stereo Processing by Semi-Global Matching and Mutual Information, IEEE Transactions on Pattern Analysis and Machine Intelligence, 30, 328-341.

Hirschmüller H. (2005). Accurate and Efficient Stereo Processing by Semi-Global Matching and Mutual Information, in Proceedings, IEEE Conference on Computer Vision and Pattern Recognition, June 2005, San Diego, CA, USA, 2, 807-814.

Hoek E. and Brown E.T. (1980). Empirical strength criterion for rock masses. J. Geotech. Engin. Div., ASCE, 106, GT9, 1013-1035.

Hoek E., Carranza-Torres C.T., Corkum B. (2002). Hoek-Brown failure criterion-2002 edition. In: Proc. of the 5th North American Rock Mechanics Symposium, Toronto, Canada. 1, 267–73.

Hungr O., Leroueil S., Picarelli L. (2014) . The Varnes Classification of Landslide Types, an Update. Landslides, 11, 167-194. Landslides. 11, 167–194.

ISPRA (2016). Report attività svolte da ISPRA in data 25-26/08/2016, 22 pp (in Italian).

Kallimogiannis V., Saroglou C. (2019). 2D and 3D 2D and 3D Back-analysis of a landslide in Egremnoi caused by the November 17 2015 Lefkada earthquake, 2nd Int. Conf. on Natural Hazards and Infrastructure, Chania, Greece.

Keefer, D.K. (1984). Landslides Caused by Earthquakes. Geological Society of America Bulletin, 95, 406–421.

Lanzo G., Tommasi P., Ausilio E. et al. (2019). Reconnaissance of geotechnical aspects of the 2016 Central Italy earthquakes. Bull Earthquake Eng 17, 5495–5532. https://doi.org/10.1007/s10518-018-0350-8

Lavecchia G., et al. (2016), Ground deformation and source geometry of the 24 August 2016 Amatrice earth-quake (Central Italy) investigated through analytical and numerical modeling of DInSAR measurements and structural-geological data, Geophys. Res. Lett., 43, 12,389 –12,398, doi:10.1002/2016GL071723

Londe P., Vigier G., Vormeringer R. (1969). Stability of rock slopes, a three-dimensional study. J. of Soil Mech and Found Div, ASCE, 95 (SM1), 235-262

Lowe D.G. (2004). Distinctive image features from scale-invariant keypoints, International Journal of Computer Vision, 60, 91-110.

Luo J., Pei X., Evans S., G., Huang R. (2019). Mechanics of the earthquake-induced Hongshiyan landslide in the 2014 M_w 6.2 Ludian earthquake, Yunnan, China. Engineering Geology, 251, 197-213.

Marr D.H., Nishihara K. (1978). Representation and recognition of the spatial organization of three-dimensional shapes. Proc. R. Soc. Lond. B. 200, 269-294.

Martino, S. Bozzano, F., Caporossi, P., D'Angiò, D., Della Seta, M., Esposito, C., Fantini, A., Fiorucci, M., Giannini, L.M., Iannucci, R., Marmoni, G.M, Mazzanti, P., Missori, C., Moretto, S., Rivellino, S., Romeo, R.W, Sarandrea, P., Schilirò, L., Troiani, F., Varone, C. (2017). Ground Effects triggered by the 24th August 2016, M_w 6.0 Amatrice (Italy) earthquake: Surveys and inventorying to update the CEDIT catalogue. Geografia Fisica e Dinamica Quaternaria, 40, 1, 77-95.

Massey et al. (2014). Determining Rockfall Risk in Christchurch Using Rockfalls Triggered by the 2010-2011 Canterbury Earthquake Sequence, Earth. Spectra, Volume 30, No. 1, pages 155-181.

Miano A., Jalayer F., Forte G., Santo A. (2020). Empirical fragility assessment using conditional GMPE-based ground shaking fields: application to damage data for 2016 Amatrice earthquake. Bulletin of Earthquake Engineering, 18(15), 6629 – 6659.

Miller R.P. (1965). Engineering Classification and Index Properties for Intact Rock. Ph. D. Thesis, Univ. Illinois.

Pierantoni, P., Deiana, G., Galdenzi, S. (2013). Stratigraphic and structural features of the Sibillini mountains (Umbria-Marche Apennines, Italy). Ital. J. Geosci. 132 (3), 497-520. https://doi.org/10.3301/IJG.2013.08.

Pizzi, A., Galadini, F. (2009). Pre-existing cross-structures and active fault segmentation in the northern-central Apennines (Italy). Tectonophysics, 476, 1–2, 304-319.

Quattrocchi F., Pik R., Pizzino L., Guerra M., Scarlato P., Angelone M., Barbieri M., Conti A., Marty B., Sacchi E., Zuppi G.M., Lombardi, S. (2000). Geochemical changes at the Bagni di Triponzo thermal spring during the Umbria-Marche 1997–1998 seismic sequence. Journal of Seismology, 4, 567–587.

Rathje E.M., Abrahamson N.A., Bray J.D., (1998). Simplified frequency content estimates of earthquake ground motions. J. Geotech. Geoenv. Eng., 124 (2), https://doi.org/10.1061/(ASCE)1090-0241(1998)124:2(150).

Rodriguez C., Bommer J., Chandler R. (1999). Earthquake-induced landslides: 1980–1997. Soil Dyn. Earthq. Eng., 18, 325-346.

Romeo, S., Di Matteo, L., Melelli, L., Cencetti, C., Dragoni, W., Fredduzzi, A. (2017). Seismic-induced rockfalls and landslide dam following the October 30, 2016 earthquake Central Italy. Landslides, 14, 1457–1465.

Rovida A., Locati M., Camassi R., Lolli B., Gasperini P. (2019). Catalogo Parametrico dei Terremoti Italiani (CPTI15), versione 2.0. Istituto Nazionale di Geofisica e Vulcanologia (INGV). https://doi.org/10.13127/CPTI/CPTI15.2

Scognamiglio L., Tinti E., Casarotti E., Pucci S., Villani F., Cocco M., et al. (2018). Complex fault geometry andrupture dynamics of the M_w 6.5, 30October 2016, central Italy earthquake. Journal of Geophysical Research: Solid Earth, 123. https://doi.org/10.1002/2018JB015603

Sepúlveda S.A., Serey A., Lara M., Pavez A., Rebolledo S. (2010). Landslides induced by the April 2007 Aysén Fjord earthquake, Chilean Patagonia. Landslides. 7, 483–492.

SGA (2000). Fenomeni franosi in Italia indotti da terremoti (sec. XIII-XX). CNR research contract 99.00152.42, unpublished report, 137 pp.

Silvestri F., Forte G., Calvello M. (2016). Multi-level approach for zonation of seismic slope stability: experiences and perspectives in Italy. In: Aversa S., Cascini L., Picarelli L., Scavia C. (eds.). Landslides and Engineered Slopes, Experience, Theory and Practice, vol. 1, 101-118, CRC Press, Leiden.

Snavely N., Seitz S.M., Richard Szeliski R. (2008). Modeling the World from Internet Photo Collections. International Journal of Computer Vision 80(2):189-210.

Tinti, E., Scognamiglio, L., Michelini, A., Cocco, M. (2016). Slip heterogeneity and directivity of the ML 6.0, 2016, Amatrice earthquake estimated with rapid finite-fault inversion. Geophysical Research Letters, 43, 10,745–10,752. https://doi.org/10.1002/2016GL071263

Tiwari B., Ajmera B., Dhital S. (2017). Characteristics of moderate- to large-scale landslides triggered by the M_w 7.8 2015 Gorkha earthquake and its aftershocks. Landslides. 14, 1297–1318.

Tommasi P., Di Giulio A., Santo A., Forte G., De Falco M., Verrucci L., Lanzo G., Rotonda T., Franke K.W. (2019). Effects of the Central Italy 2016 seismic sequence on slope stability: preliminary analysis of

some major rock slides. In Silvestri & Moraci (eds.) Earthquake Geotechnical Engineering for Protection and Development of Environment and Costructions.

Verrucci L., Forte G., Di Giulio A., De Falco M., Tommasi P., Lanzo G., Franke K., Santo A. (2021). Pseudo-static back-analysis of major rock-slides occurred during the 2016-2017 central Italy seismic sequence. Companion paper submitted to Engineering Geology

Xu C., Xu X., Shyu J.B. H., Gao M., Tan X., Ran Y., Zheng W. (2015). Landslides triggered by the 20 April 2013 Lushan, China, M_w 6.6 earthquake from field investigations and preliminary analyses. Landslides. 12, 365–385.

CAPTIONS

Fig. 1. Epicentres of the 2016-2017 Central Italy seismic sequence (from INGV http://terremoti.ingv.it/, last accessed March 30th 2020) and location of the triggered landslides.

Fig. 2. Earthquake triggered landslides in the study area. **a)** Simplified geological sketch of the study area with distribution of the landslides triggered by historical (1997; 2009) and recent (2016) seismic events (Modified after **Forte et al., 2019**). Keys: CB Carbonate Bedrock; McB Marly Carbonate Bedrock; AFB Arenaceous Flysch Bedrock; CFB Clayey Flysch Bedrock; CgB Conglomerate Bedrock; tv Travertine; db Debris; tcg terraced conglomerates; gs gravels and sands. GLF Gorzano – Laga Fault; VBF Vettore – Bove Fault. **b) Keefer** (**1984**) diagram for Category I of the collected rockfalls.

Fig. 3. Digital surface model views of the scar areas for the studied rock slides: **a)** Nera (NR); **b)** Costa Cattiva (CC); **c)** Piè La Rocca (PR); **d)** Rubbiano (RB).

Fig. 4. Plot of Schmidt hammer rebound height, R_L, vs. uniaxial compression strength *UCS*.

Fig. 5. Nera rock slide; **a)** Local geological setting reporting faults and morphostructural features, (http://dati.umbria.it/dataset/carta-geologica-dell-umbria and https://www.regione.marche.it/Regione-Utile/Paesaggio-Territorio-Urbanistica/Cartografia/); **b)** 3D geostructural model highlighting the discontinuity sets; **c)** stereoplot with Fisher concentrations of poles and related great circles (colours of each set are the same of joint surfaces in Fig. b).

Fig. 6. Costa Cattiva rock slide; **a)** Local geological setting reporting faults and morphostructural features, (http://dati.umbria.it/dataset/carta-geologica-dell-umbria and https://www.regione.marche.it/Regione-Utile/Paesaggio-Territorio-Urbanistica/Cartografia/); **b)** 3D geostructural model highlighting the discontinuity sets; **c)** stereoplot with Fisher concentrations of poles and related great circles (colours of each set are the same of joint surfaces in Fig. b).

Fig. 7. Piè La Rocca rock slide; **a)** Local geological setting reporting faults and morphostructural features, (http://dati.umbria.it/dataset/carta-geologica-dell-umbria and https://www.regione.marche.it/Regione-Utile/Paesaggio-Territorio-Urbanistica/Cartografia/); **b)** 3D geostructural model highlighting the discontinuity sets; **c)** stereoplot with Fisher concentrations of poles and related great circles (colours of each set are the same of joint surfaces in Fig. b).

Fig. 8. Rubbiano rock-slide; **a)** Local geological setting reporting faults and morphostructural features, (https://www.regione.marche.it/Regione-Utile/Paesaggio-Territorio-Urbanistica/Cartografia); **b)** 3D geostructural model highlighting the discontinuity sets; different colours represent joint surfaces belonging to each set reported in the **c)** Fisher concentration stereoplot.

Fig. 9. Rosette and stereoplots of the studied landslides: **a-b)** Nera (NR); **c-d)** Costa Cattiva (CC); **e-f)** Pié La Rocca (PR); **g-h)** Rubbiano (RB).

Fig. 10. Oblique photograph of joint surface J2 from the 3D point cloud. Pale patch indicated by arrows correspond to rock bridges. The direction of sight has been rotated to better show the joint surface.

Fig. 11. Simplified geometrical models of the rock slides triggered by the Central Italy Earthquakes. **a)** Nera (NR), the white irregular surface contoured with a dashed line corresponds to a possible failure through the intact rock mass; **b)** Costa Cattiva (CC); **c)** Pié La Rocca (PR); **d)** Rubbiano (RB).

Fig. 12. Stereographic conform projections (lower hemisphere projected from upper focal point) of the triangular regions (solid lines) that define different sliding mechanisms depending on the direction of the external resultant force (red circles). *Iij*= sliding along the intersection line between the planes *i* and *j*, *pi*=sliding along the plane *i*, *no*= region of impossible motion, *0* = region of complete detachment from all joints. Light dotted lines represent the average local slope face.

TABLES

Table 1. Main shocks and high-magnitude aftershocks of the Central Italy seismic sequence.

Epicentre	Date	Time GMT	*Mw*	Epicentre			Orientation		Extent (a×b)*
				Lat.	Long.	Depth	Strike	Dip	(km)
-		hh:mm:ss	-	(°)	(°)	(km)	(°)	(°)	13.5x7
Accumoli (RI)	2016-08-24	01:36:32	6.0	42.70	13.23	8.0	155	49	-
Norcia (PG)	2016-08-24	02:33:29	5.3	42.79	13.15	8.0	135	47	-
Castelsantangelo (MC)	2016-10-26	21:18:07	5.4	42.88	13.12	8.0	161	38	-
Visso (MC)	2016-10-26	21:18:07	5.9	42.91	13.09	10.0	159	47	8×4
Norcia (PG)	2016-10-30	06:40:18	6.5	42.84	13.11	10.0	151	47	21×16
Capitignano (AQ)	2017-01-18	11:14:09	5.5	42.53	13.28	10.0	161	51	-
Capitignano(AQ)	2017-01-18	11:25:23	5.4	42.50	13.28	9.0	319	55	-

* Length (a), along-dip width (b) (**GEER, 2017**).

Table 2. Main features of the investigated rock slides

Landslide	Lat (°)	Lon (°)	Estimated volume ($m^3 \cdot 10^3$)	Lithology	Triggering earthquake	Epicentral distance (km)	Peak acceleration (g)	Mean period (s)	Significant duration (s)
Nera (NR) (Sasso Pizzuto Mt.)	42.93	13.07	32.0	*Maiolica Fm.*	10/30/2016, *Mw* 6.5	10.3	0.310	0.529	8.04
Costa Cattiva (CC) (Nera River Valley)	42.92	13.12	0.4	*Maiolica Fm.*	10/30/2016, *Mw* 5.9 10/30/2016, *Mw* 5.4	2.3 4.4	0.166 0.232	0.398 0.366	11.09 3.04
Piè La Rocca (PR) (Patino Mt.)	42.82	13.13	15.0	*Calcare Massiccio Fm.*	08/24/2016, *Mw* 6.0 08/24/2016, *Mw* 5.3	14.9 4.5	0.055 0.158	0.840 0.251	12.08 16.56
Rubbiano (RB) (Infernaccio gorge)	42.93	13.28	15.0	*Maiolica Fm.*	10/30/2016, *Mw* 6.5	16.8	0.260	0.529	8.04

Table 3. Mean values of the physical and mechanical properties of the intact rock

Lithotype	*GSI* -	ρ_d (Mg/m^3)	ρ_s (Mg/m^3)	*n* (%)	V_P (km/s)	V_S (km/s)	*UCS* (MPa)	σ_t (MPa)	m_i -
Maiolica Fm.	52 (CC,NR) 45-60 (RB)	2.65	2.72	2.7	6.0	2.9	53	4.0	8
Calcare Massiccio Fm.	52-65 (PR)	2.68	2.75	2.5	6.1	3.2		4.5	

ρ_d: bulk dry density; ρ_s: density of the solid matrix; *n*: porosity; V_P/V_S: longitudinal/shear wave velocity; σ_t: indirect tensile strength; *UCS*: uniaxial compression strength; m_i: Hoek-Brown strength parameter (from tests on specimens from a neighbouring location)

Table 4. Input parameters and results for the static stability analyses

Rock slide	Volume (m^3)	Plane 1			Plane 2			Plane 3	Sliding mechanism	Factor of safety F_S
		dip/dd (°)	φ_1' (°)	$A_{p1}+A_{b1}$ (m^2)	dip/dd (°)	φ_2' (°)	A_{b2} (m^2)	dip/dd (°)		
NR	30940	77/337	47	570 + 0	60/270	40	0	48/95	line I_{12}	0.93-2.16*
»	»	»	»	570 + 800	»	»	»	»	»	1.00-2.23*
CC	400	75/330	47	0	35/090	40	0	-	line I_{12}	2.16
PR	14000	75/330	47	0	40/255	42	0	72/106	on plane 2	1.07
RB	15000	65/084	47	0	85/130	40	2880	-	on plane 1	1.11**

dd: dip direction

*: the range correspond to a variation of the cohesion of rock bridges between 0.53 and 2 MPa

**: with the tensile contribution of the rear wedge surface (plane 2, composite surface)

Highlights

- 3D Rockslides models were obtained from UAV surveys
- Structure from Motion (SfM) permitted to characterize the discontinuty sets
- The tectonic pattern of the area is controlled by NW-SE Quaternary faults
- Rockslides are locally controlled by more ancient discontinuity systems
- Failures of rock bridges were involved in the sliding